PHYSICAL REVIEW D **77,** 114023 (2008)

Finite-Q^2 corrections to parity-violating DIS

T. Hobbs
The University of Chicago, 5801 South Ellis Avenue, Chicago, Illinois 60637, USA

W. Melnitchouk
Jefferson Lab, 12000 Jefferson Avenue, Newport News, Virginia 23606, USA
(Received 30 January 2008; published 26 June 2008)

Parity-violating deep inelastic scattering (PVDIS) has been proposed as an important new tool to extract the flavor and isospin dependence of parton distributions in the nucleon. We discuss finite-Q^2 effects in PVDIS asymmetries arising from subleading kinematical corrections and longitudinal contributions to the γZ interference. For the proton, these need to be accounted for in order to accurately extract the d/u ratio at large x; for the deuteron they are important to consider when searching for evidence of charge symmetry violation in parton distributions or signals for physics beyond the standard model. We further explore the dependence of PVDIS asymmetries for polarized targets on the u and d helicity distributions at large x.

DOI: 10.1103/PhysRevD.77.114023 PACS numbers: 13.60.Hb, 11.30.Er, 12.38.−t

I. INTRODUCTION

The scattering of highly energetic leptons from nucleon targets has over the years provided a wealth of information on the nucleon quark and gluon (or parton) substructure. Most of the information has come from electromagnetic deep inelastic scattering (DIS) of electrons (or muons), while neutrino DIS has yielded complementary constraints on valence and sea parton distribution functions (PDFs) via the weak current.

A relatively unexplored method of measuring PDFs is through the interference of electromagnetic and weak currents, which in principle selects a unique combination of quark flavors. This involves measuring the small $\gamma - Z^0$ interference amplitude in the neutral current DIS of a polarized electron from a hadron h, $\vec{e}h \to eX$. Because the axial current is sensitive to the polarization of the incident electron, measurement of the asymmetry between left- and right-hand polarized electrons is proportional to the $\gamma - Z^0$ interference amplitude.

In fact, in the 1970s parity-violating deep inelastic scattering (PVDIS) on the deuteron provided an important early confirmation of the standard model of particle physics [1,2]. Three decades on, experimental techniques are sophisticated enough now to enable left-right asymmetries to be measured to a few parts per million, and current facilities will be able to improve the statistics of the earlier experiments by an order of magnitude [3,4].

For parity-violating scattering from an isoscalar deuteron, the dependence of the left-right asymmetry on PDFs cancels in the parton model, so that the asymmetry is determined entirely by the Weinberg angle, θ_W. In the SU(2) × U(1) electroweak theory, the Lagrangian corresponding to the parity-violating (PV) lepton-quark interaction (for two quark flavors) is given by [5,6]

$$\mathcal{L}^{\mathrm{PV}} = \frac{G_F}{\sqrt{2}}[\bar{e}\gamma^\mu\gamma_5 e(C_{1u}\bar{u}\gamma_\mu u + C_{1d}\bar{d}\gamma_\mu d) + \bar{e}\gamma^\mu e(C_{2u}\bar{u}\gamma_\mu\gamma_5 u + C_{2d}\bar{d}\gamma_\mu\gamma_5 d)], \quad (1)$$

where G_F is the Fermi coupling constant, and the electroweak couplings at tree level are

$$C_{1u} = g_A^e \cdot g_V^u = -\tfrac{1}{2} + \tfrac{4}{3}\sin^2\theta_W, \quad (2a)$$
$$C_{1d} = g_A^e \cdot g_V^d = \tfrac{1}{2} - \tfrac{2}{3}\sin^2\theta_W, \quad (2b)$$
$$C_{2u} = g_V^e \cdot g_A^u = -\tfrac{1}{2} + 2\sin^2\theta_W, \quad (2c)$$
$$C_{2d} = g_V^e \cdot g_A^d = \tfrac{1}{2} - 2\sin^2\theta_W. \quad (2d)$$

With our conventions the vector and axial-vector couplings of the charged lepton are $g_V^e = -1 + 4\sin^2\theta_W$ and $g_A^e = +1$, respectively. The vector couplings of the quarks are given by $g_V^u = -1/2 + (4/3)\sin^2\theta_W$ and $g_V^d = 1/2 - (2/3)\sin^2\theta_W$, while the quark axial-vector couplings are $g_A^u = 1/2$ and $g_A^d = -1/2$, respectively. The deuteron asymmetry is therefore a sensitive test of effects beyond the parton model, such as higher twist contributions, or of more exotic effects such as charge-symmetry violation in PDFs or new physics beyond the standard model.

More recently it has been suggested that PVDIS can be used to probe parton distribution functions in the largely unmeasured region of high Bjorken-x [7,8]. In particular, the PVDIS asymmetry for a proton is proportional to the ratio of d to u quark distributions at large x. Current determinations of the d/u ratio rely heavily on inclusive proton and deuteron DIS data, and there are large uncertainties in the nuclear corrections in the deuteron at high x [9]. While novel new methods have been suggested to minimize the nuclear uncertainties [10–12], the use of a proton target alone would avoid the problem altogether.

In this paper we critically examine the accuracy of the parton model predictions for the PVDIS asymmetries in

realistic experimental kinematics at finite Q^2. In particular, in Sec. II we provide a complete set of formulas for cross sections and asymmetries for scattering polarized leptons from unpolarized targets, including finite-Q^2 effects. PVDIS from the proton is discussed in Sec. III, where we test the sensitivity of the extraction of the d/u ratio at large x to finite-Q^2 corrections. One of the main uncertainties in the calculation is the ratio of longitudinal to transverse cross sections for the $\gamma - Z^0$ interference, for which no empirical information currently exists. We provide some numerical estimates of the possible dependence of the left-right asymmetry on this ratio.

For deuteron targets, we examine in Sec. IV how the asymmetry is modified in the presence of finite-Q^2 corrections, and where these can pose significant backgrounds for extracting standard model signals. Finally, we explore in Sec. V the possibility of using PVDIS with polarized targets to constrain quark helicity distributions at large x. A comprehensive discussion of polarized PVDIS in the parton model was previously given by Anselmino *et al.* [13]; here we perform a numerical survey of the sensitivity of polarized PVDIS asymmetries to spin-dependent PDFs. In Sec. VI we make concluding remarks and outline future work.

II. PARITY-VIOLATING DEEP INELASTIC SCATTERING

In this section we outline the formalism relevant for parity-violating deep inelastic scattering of an electron (four-momentum l) from a nucleon target (p) to a scattered electron (l') and hadronic debris (p_X), via the exchange of a virtual photon or Z^0-boson (q). We discuss the general decomposition of the hadronic tensor and provide formulas for the PV asymmetry in terms of structure functions and in the parton model in terms of PDFs.

A. Hadronic tensor

We begin with the differential cross section for inclusive electron-nucleon scattering, which in general can be written as the squared sum of the γ- and Z^0-exchange amplitudes. We will consider contributions to the cross section from the pure γ exchange amplitude and the γ-Z interference; the purely weak Z^0 exchange contribution to the cross section is strongly suppressed relative to these and can be neglected.

Formally, the cross section can be written in terms of products of leptonic and hadronic tensors as [13,14]

$$\frac{d^2\sigma}{d\Omega dE'} = \frac{\alpha^2}{Q^4}\frac{E'}{E}\left(L^{\gamma}_{\mu\nu}W^{\mu\nu}_{\gamma} + \frac{G_F}{4\sqrt{2}\pi\alpha}L^{\gamma Z}_{\mu\nu}W^{\mu\nu}_{\gamma Z}\right), \quad (3)$$

where E and E' are the (rest frame) electron energies, Q^2 is (minus) the four-momentum transfer squared, and α is the electromagnetic fine structure constant. The lepton tensor for the interference current in Eq. (3) is given by

$$L^{\gamma Z}_{\mu\nu} = (g^e_V + \lambda g^e_A)L^{\gamma}_{\mu\nu}, \quad (4)$$

with $\lambda = +1(-1)$ for positive (negative) initial lepton helicity, and the purely electromagnetic tensor is given by

$$L^{\gamma}_{\mu\nu} = 2(l_\mu l'_\nu + l'_\mu l_\nu - l\cdot l' g_{\mu\nu} + i\lambda\varepsilon_{\mu\nu\alpha\beta}l^\alpha l'^\beta). \quad (5)$$

The hadronic tensors for the electromagnetic and interference contributions are given by

$$W^{\gamma(\gamma Z)}_{\mu\nu} = \frac{1}{2M}\sum_X \{\langle X|J^{\gamma(Z)}_\mu|N\rangle^*\langle X|J^{\gamma}_\nu|N\rangle + \langle X|J^{\gamma}_\mu|N\rangle^*\langle X|J^{\gamma(Z)}_\nu|N\rangle\}(2\pi)^3\delta(p_X - p - q), \quad (6)$$

where M is the nucleon mass, and $J^{\gamma(Z)}_\mu$ is the electromagnetic (weak) hadronic current. In general, the hadronic tensor for a nucleon with spin four-vector S^μ can be written in terms of 3 spin-independent and 5 spin-dependent structure functions [13]:

$$\begin{aligned} W^i_{\mu\nu} = &-\frac{g_{\mu\nu}}{M}F^i_1 + \frac{p_\mu p_\nu}{Mp\cdot q}F^i_2 + \frac{i\varepsilon_{\mu\nu\alpha\beta}p^\alpha q^\beta}{2Mp\cdot q}F^i_3 \\ &+ \frac{i\varepsilon_{\mu\nu\alpha\beta}}{p\cdot q}(q^\alpha S^\beta g^i_1 + 2xp^\alpha S^\beta g^i_2) \\ &- \frac{p_\mu S_\nu + S_\mu p_\nu}{2p\cdot q}g^i_3 + \frac{S\cdot q p_\mu p_\nu}{(p\cdot q)^2}g^i_4 \\ &+ \frac{S\cdot q g_{\mu\nu}}{p\cdot q}g^i_5, \end{aligned} \quad (7)$$

for both the electromagnetic ($i = \gamma$) and interference ($i = \gamma Z$) currents. Each of the structure functions generally depend on two variables, usually taken to be Q^2 and the Bjorken scaling variable $x = Q^2/2M\nu$, where ν is the energy transfer.

Below we will consider scattering of a polarized electron from an unpolarized hadron target, in which only the spin-independent structure functions $F^{\gamma Z}_{1-3}$ enter. Asymmetries resulting from scattering of an unpolarized-electron beam from a polarized target, which are sensitive to the spin-dependent structure functions $g^{\gamma Z}_{1-5}$, will be discussed in Sec. V.

B. Beam asymmetries

The PV interference structure functions can be isolated by constructing an asymmetry between cross sections for right- (σ_R) and left-hand (σ_L) polarized electrons:

$$A^{\rm PV} = \frac{\sigma_R - \sigma_L}{\sigma_R + \sigma_L}, \quad (8)$$

where $\sigma \equiv d^2\sigma/d\Omega dE'$. Since the purely electromagnetic and purely weak cross sections do not contribute to the asymmetry for $Q^2 \ll M_Z^2$, the numerator is sensitive only to the γ-Z interference term. The denominator, on the other hand, is dominated by the purely electromagnetic component. In terms of structure functions, the PVDIS asymmetry can be written

$$A^{\rm PV} = -\left(\frac{G_F Q^2}{4\sqrt{2}\pi\alpha}\right)\frac{g_A^e(2xyF_1^{\gamma Z} - 2[1 - 1/y + xM/E]F_2^{\gamma Z}) + g_V^e x(2-y)F_3^{\gamma Z}}{2xyF_1^{\gamma} - 2[1 - 1/y + xM/E]F_2^{\gamma}}, \tag{9}$$

where $y = \nu/E$ is the lepton fractional energy loss.

In the Bjorken limit (Q^2, $\nu \to \infty$, x fixed), the interference structure functions $F_1^{\gamma Z}$ and $F_2^{\gamma Z}$ are related by the Callan-Gross relation, $F_2^{\gamma Z} = 2xF_1^{\gamma Z}$, similar to the electromagnetic $F_{1,2}^{\gamma}$ structure functions [13]. At finite Q^2, however, corrections to this relation are usually parameterized in terms of the ratio of the longitudinal to transverse virtual photon cross sections:

$$R^{\gamma(\gamma Z)} \equiv \frac{\sigma_L^{\gamma(\gamma Z)}}{\sigma_T^{\gamma(\gamma Z)}} = r^2\frac{F_2^{\gamma(\gamma Z)}}{2xF_1^{\gamma(\gamma Z)}} - 1, \tag{10}$$

for both the electromagnetic (γ) and interference (γZ) contributions, with

$$r^2 = 1 + \frac{Q^2}{\nu^2} = 1 + \frac{4M^2x^2}{Q^2}. \tag{11}$$

In terms of this ratio, the PVDIS asymmetry can be written more simply as

$$A^{\rm PV} = -\left(\frac{G_F Q^2}{4\sqrt{2}\pi\alpha}\right)\left[g_A^e Y_1\frac{F_1^{\gamma Z}}{F_1^{\gamma}} + \frac{g_V^e}{2}Y_3\frac{F_3^{\gamma Z}}{F_1^{\gamma}}\right], \tag{12}$$

where the functions $Y_{1,3}$ parameterize the dependence on y and on the R ratios:

$$Y_1 = \frac{1 + (1-y)^2 - y^2(1 - r^2/(1+R^{\gamma Z})) - 2xyM/E}{1 + (1-y)^2 - y^2(1 - r^2/(1+R^{\gamma})) - 2xyM/E}\left(\frac{1+R^{\gamma Z}}{1+R^{\gamma}}\right), \tag{13a}$$

$$Y_3 = \frac{1 - (1-y)^2}{1 + (1-y)^2 - y^2(1 - r^2/(1+R^{\gamma})) - 2xyM/E}\left(\frac{r^2}{1+R^{\gamma}}\right). \tag{13b}$$

In the Bjorken limit, the kinematical ratio $r^2 \to 1$, while the longitudinal cross section vanishes relative to the transverse, $R^i \to 0$, for both $i = \gamma$ and γZ. For kinematics relevant to future experiments ($Q^2 \sim$ few GeV^2, $\nu \sim$ few GeV), the factor $2xyM/E$ provides a small correction and can for practical purposes be dropped. In this case the functions Y_1 and Y_3 have the familiar limits [1]:

$$Y_1 \to 1, \tag{14a}$$

$$Y_3 \to \frac{1 - (1-y)^2}{1 + (1-y)^2} \equiv f(y). \tag{14b}$$

Typically the contribution from the Y_3 term is much smaller than from the Y_1 term because $g_V^e \ll g_A^e$, although for quantitative comparisons it needs to be included.

C. Electroweak structure functions

The PVDIS asymmetry $A^{\rm PV}$ can be evaluated from knowledge of the electromagnetic and interference structure functions. At leading twist of the electroweak structure functions can be expressed in terms of PDFs. For reference these are listed (at leading order in α_s) as follows:

$$F_1^{\gamma}(x) = \frac{1}{2}\sum_q e_q^2(q(x) + \bar{q}(x)), \tag{15a}$$

$$F_2^{\gamma}(x) = 2xF_1^{\gamma}(x), \tag{15b}$$

for the pure electromagnetic case, while

$$F_1^{\gamma Z}(x) = \sum_q e_q g_V^q(q(x) + \bar{q}(x)), \tag{16a}$$

$$F_2^{\gamma Z}(x) = 2xF_1^{\gamma Z}(x), \tag{16b}$$

$$F_3^{\gamma Z}(x) = 2\sum_q e_q g_A^q(q(x) - \bar{q}(x)), \tag{16c}$$

are the structure functions for the weak-electromagnetic interference, where the quark q and antiquark $\bar{q}$ distributions are defined with respect to the proton.

In terms of PDFs, the PV asymmetry in Eq. (12) can be written as

$$A^{\rm PV} = -\left(\frac{G_F Q^2}{4\sqrt{2}\pi\alpha}\right)(Y_1 a_1 + Y_3 a_3), \tag{17}$$

where the vector term a_1 is given by

$$a_1 = \frac{2\sum_q e_q C_{1q}(q + \bar{q})}{\sum_q e_q^2(q + \bar{q})}, \tag{18a}$$

while the axial-vector term is

$$a_3 = \frac{2\sum_q e_q C_{2q}(q - \bar{q})}{\sum_q e_q^2(q + \bar{q})}. \tag{18b}$$

In this analysis we will focus on the large-x region dominated by valence quarks, so that the effects of sea quark will be negligible.

At finite Q^2, corrections to the parton model expressions appear in the form of perturbatively generated α_s correc-

tions, target mass corrections [15], as well as higher twist ($1/Q^2$ suppressed) effects. Some higher twist effects in PVDIS have previously been investigated in the literature [16]. One should also note that at large x perturbative calculations beyond leading order can become unstable and threshold resummations need to be performed [17].

A detailed study of each of these corrections will be published elsewhere [18]; in the present study we focus on the finite-Q^2 effects on the asymmetry arising from nonzero values of $R^{\gamma(\gamma Z)}$, which to date have not been considered. While data and phenomenological parametrizations are available for R^γ [19–21], currently no empirical information exists on $R^{\gamma Z}$. In our numerical estimates below, we shall consider a range of possible behaviors for $R^{\gamma Z}$ and examine its effect on $A^{\rm PV}$.

III. PVDIS ON THE PROTON

Parity-violating DIS on a proton target has recently been discussed as a means of constraining the ratio of d to u quark distributions at large x [7]. At present the d/u ratio is essentially unknown beyond $x \sim 0.6$ due to large uncertainties in the nuclear corrections in the deuteron, which is the main source of information on the d quark distribution [9,12]. Several new approaches to determining d/u at large x have been proposed, for example, using spectator proton tagging in semi-inclusive DIS from the deuteron [11], or through a ratio of ^{3}He and ^{3}H targets to cancel the nuclear corrections [10]. The virtue of the PVDIS method is that, rather than using different hadrons (or nuclei) to select different flavors, here one uses (the interference of) different gauge bosons to act as the flavor filter, thereby avoiding nuclear uncertainties altogether.

In the valence region at large x, the PV asymmetry is sensitive to the valence u and d quark distributions in the proton. Here the functions a_1 and a_3 in Eqs. (18) for the proton can be simplified to

$$a_1^p = \frac{12C_{1u} - 6C_{1d}d/u}{4 + d/u}, \tag{19a}$$

and

$$a_3^p = \frac{12C_{2u} - 6C_{2d}d/u}{4 + d/u}. \tag{19b}$$

This reveals that both a_1^p and a_3^p depend on the d/u quark distribution ratio.

To explore the relative sensitivity of the proton asymmetry $A_p^{\rm PV}$ to the vector and axial-vector terms, in Fig. 1 we show the functions Y_1 and Y_3 for the proton as a function of x, evaluated at $Q^2 = 5$ GeV^2, for a beam energy $E = 10$ GeV (which we will assume throughout). For Y_1, the solid line (at $Y_1 = 1$) corresponds to $R^{\gamma Z} = R^\gamma$, while the dashed (dotted) curves around it represent $+(-)20\%$ deviations of $R^{\gamma Z}$ from R^γ (see below). For Y_3, the Bjorken-limit result ($R^\gamma = 0$, $r^2 = 1$) is given by the dotted curve,

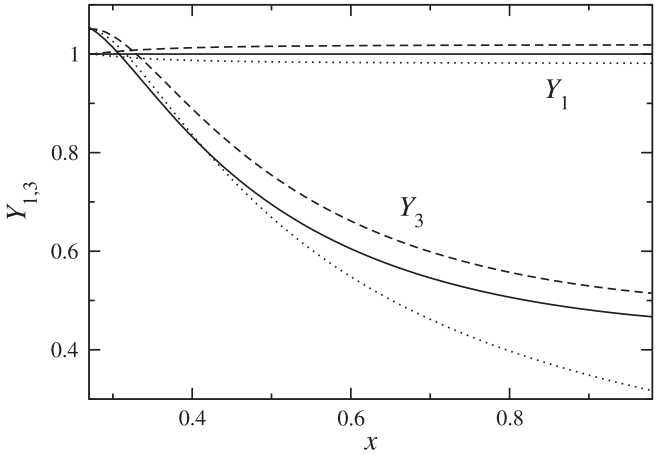

FIG. 1. Y_1 and Y_3 as a function of x, for $Q^2 = 5$ GeV^2 and $E = 10$ GeV. For Y_1, the solid line (at $Y_1 = 1$) corresponds to $R^{\gamma Z} = R^\gamma$ [19], while the dashed (dotted) curves around it represent $+(-)20\%$ deviations of $R^{\gamma Z}$ from R^γ. For Y_3, the Bjorken-limit result ($R^\gamma = 0$, $r^2 = 1$) is given by the dotted curve, the dashed curve has $R^\gamma = 0$ but $r^2 \neq 1$, while the solid curve represents the full result.

the dashed curve has $R^\gamma = 0$ but $r^2 \neq 1$, while the solid curve represents the full result with $R^\gamma \neq 0$ and $r^2 \neq 1$. In all cases we use R^γ from the parametrization of Ref. [19]. The results with the parametrization of Ref. [20] are very similar, and are consistent within the quoted uncertainties.

Note that at fixed Q^2, the large-x region also corresponds to low hadronic final state masses W, so that with increasing x one eventually encounters the resonance region at $W \lesssim 2$ GeV. For $Q^2 = 5$ GeV^2 this occurs at $x \approx 0.62$, and for $Q^2 = 10$ GeV^2 at $x \approx 0.76$. This may introduce an additional source of uncertainty in the extraction of the PV asymmetry at large x, arising from possible higher twist corrections to structure functions. In actual experimental conditions, the value of Q^2 can be varied with x to ensure that the resonance region is excluded from the data analysis. For the purposes of illustrating the finite-Q^2 effects in our analysis, we shall fix Q^2 at the low end of values attainable with an energy of $E = 10$ GeV, namely, $Q^2 = 5$ GeV^2.

The relative roles played by the vector and axial-vector terms at different Q^2 values are illustrated in Fig. 2, where Y_1 and Y_3 are plotted as a function of Q^2 at a fixed $x = 0.7$. In Fig. 2(a) we show the dependence of Y_1 on the interference ratio $R^{\gamma Z}$. With $R^{\gamma Z} = R^\gamma$ the result is unity, as expected from Eq. (13a). Varying $R^{\gamma Z}$ by $\pm 20\%$ relative to R^γ [19] results in an $\approx 4\%$ shift at $Q^2 \sim 1$ GeV^2, decreasing to $<1\%$ for $Q^2 \sim 10$ GeV^2.

For the axial-vector contribution, in Fig. 2(b) we show Y_3 under various kinematical approximations, namely, in the Bjorken-limit ($R^\gamma = 0$, $r^2 = 1$), for $R^\gamma = 0$ but $r^2 \neq 1$, and the full result. The differences between the full and Bjorken-limit results are of the order 40% at $Q^2 = 5$ GeV^2 and $\sim 20\%$ at $Q^2 = 10$ GeV^2. The rise in Y_3 with Q^2 is

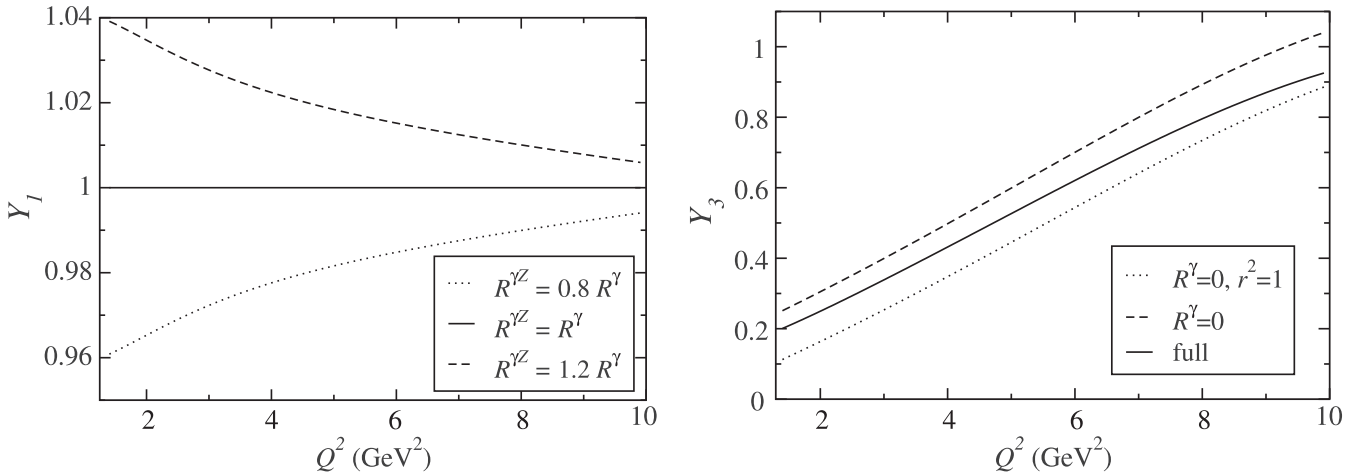

FIG. 2. Y_1 and Y_3 as a function of Q^2, for $x = 0.7$ and $E = 10$ GeV: (a) Dependence of Y_1 on $R^{\gamma Z}$, for $R^{\gamma Z} = 0.8R^{\gamma}$ (dotted curve), $R^{\gamma Z} = R^{\gamma}$ (solid curve), and $R^{\gamma Z} = 1.2R^{\gamma}$ (dashed curve). (b) Dependence of Y_3 on R^{γ}, in the Bjorken limit ($R^{\gamma} = 0$, $r^2 = 1$) (dotted curve), with $R^{\gamma} = 0$ but $r^2 \neq 1$ (dashed curve), and full result (solid curve).

kinematical, since $y \sim \nu \sim Q^2$ for fixed x and E. Because the axial contribution is suppressed relative to the vector term in $A^{\rm PV}$, $g_V^e \ll g_A^e$, the uncertainty in $A^{\rm PV}$ arising from Y_3 will be less significant. Numerically, the ratio a_3^p/a_1^p of the axial to vector terms, using the CTEQ6 [22] parametrization of the PDFs, ranges from 0.21–0.24 for $0.4 < x < 0.9$. Although the axial-vector a_3^p term is small, it is nevertheless important to take into account in precision determinations of $A_p^{\rm PV}$.

The sensitivity of the proton asymmetry $A_p^{\rm PV}$, measured in parts per million (ppm), to the d/u ratio is illustrated in Fig. 3 as a function of x, for $Q^2 = 5$ GeV^2, where $A_p^{\rm PV}/Q^2$ is shown. Here we assume that $R^{\gamma Z} = R^{\gamma}$, so that the coefficient Y_1 in the vector term is unity. For the u and d distributions we use the CTEQ6 PDF set [22], in which the d/u ratio vanishes as $x \to 1$, along with a modified d/u ratio which has a finite $x \to 1$ limit of 0.2 [9], $d/u \to d/u + 0.2x^2 \exp(-(1-x)^2)$ [23], motivated by theoretical counting rule arguments [24]. Also shown (dotted band around the CTEQ6 prediction) is a $\pm 1\%$ uncertainty, which is a conservative estimate of what may be expected experimentally at JLab with 12 GeV [4,7]. The results indicate that a signal for a larger d/u ratio would be clearly visible above the experimental errors.

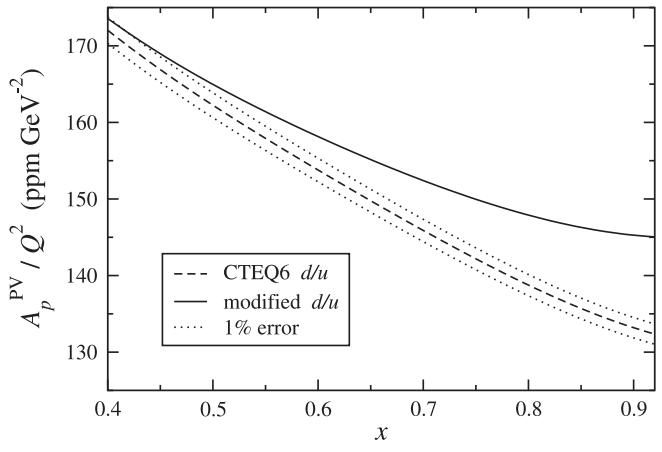

FIG. 3. Proton PV asymmetry $A_p^{\rm PV}/Q^2$ as a function of x, for $Q^2 = 5$ GeV^2, in parts per million (ppm) $\cdot$ GeV^{-2}. The prediction with the standard CTEQ6 PDFs (dashed curve) is compared with that using a modified d/u ratio at large x (solid curve). A $\pm 1\%$ uncertainty band (dotted curve) is shown around the standard CTEQ6 prediction.

At finite Q^2 the asymmetry $A_p^{\rm PV}$ depends not only on the PDFs, but also on the longitudinal to transverse cross sections ratios R^{γ} and $R^{\gamma Z}$ for the electromagnetic and γZ interference contributions, respectively. A number of measurements of the former have been taken at SLAC and JLab [19–21], and parametrizations of R^{γ} in the DIS region exist. In Fig. 4 the relative effect on $A_p^{\rm PV}$ from R^{γ} is shown via the ratio $\delta^{(R^{\gamma})}A_p^{\rm PV}/A_p^{\rm PV(0)}$, where $\delta^{(R^{\gamma})}A_p^{\rm PV} = A_p^{\rm PV} - A_p^{\rm PV(0)}$ is the difference between the full asymmetry, with nonzero values of R^{γ}, and that calculated in Bjorken-limit kinematics, $A_p^{\rm PV(0)}$.

The effect on $A_p^{\rm PV}$ from the purely kinematical r^2 correction in the Y_3 term (with $R^{\gamma} = 0$), compared with the Bjorken-limit prediction, is of the order 2%–4% over the range $0.5 \lesssim x \lesssim 0.9$. Including the R^{γ} ratio from Ref. [19] reduces the effect down to $\approx$ 1–3% over the same range, with an uncertainty of $\approx \pm 0.5\%$ for $x \lesssim 0.8$, and $\approx 1\%$ at larger x. This behavior can be easily understood from the expression for Y_3 in Eq. (13b). While the r^2 factor in the numerator of Y_3 leads to a larger asymmetry at finite Q^2 (the r^2 dependence in the denominator is in contrast diluted by the y^2 factor), a nonzero value for R^{γ} in the denominator of Eq. (13b) decreases Y_3 and lowers the overall correction.

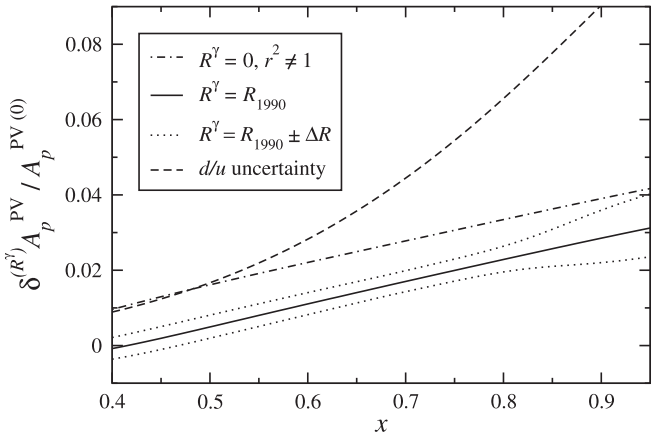

FIG. 4. Relative effects on the proton PV asymmetry $A_p^{\rm PV}$ from the electromagnetic ratio R^γ (keeping $R^{\gamma Z} = R^\gamma$), compared with the Bjorken-limit asymmetry $A_p^{\rm PV(0)}$. The full results (solid curve), for $Q^2 = 5$ GeV^2, are compared with those for $R^\gamma = 0$ (but $r^2 \neq 1$) (dotted-dashed curve), with the dotted curves representing the uncertainty on R^γ (from the "R_{1990}" parameterization of Ref. [19]). For reference the relative uncertainty in $A_p^{\rm PV}$ arising from the d/u ratio is also shown (dashed curve).

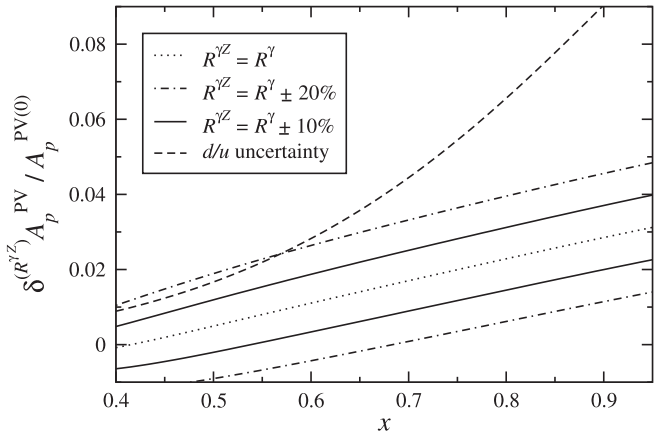

FIG. 5. Relative effects on the proton PV asymmetry $A_p^{\rm PV}$ from the γZ interference ratio $R^{\gamma Z}$ compared with the Bjorken-limit asymmetry $A_p^{\rm PV(0)}$. The baseline result for $R^{\gamma Z} = R^\gamma$ (dotted curve) is compared with the effects of modifying $R^{\gamma Z}$ by $\pm 10\%$ (solid curve) and $\pm 20\%$ (dotted-dashed curve), for $Q^2 = 5$ GeV^2. For reference the relative uncertainty $\delta^{(d/u)} A_p^{\rm PV} / A_p^{\rm PV(0)}$ from the d/u ratio is also shown (dashed curve).

These effects are to be compared with the relative change in $A_p^{\rm PV}$ arising from different large-x behaviors of the d/u ratio (dashed curve), expressed as a difference of the asymmetries with the standard CTEQ6 [22] PDFs and ones with a modified d/u ratio [9,23], $\delta^{(d/u)} A_p^{\rm PV} / A_p^{\rm PV(0)}$, where $A_p^{\rm PV(0)}$ is computed in terms of the standard (unmodified) PDFs. This is of the order 2% for $x \sim 0.5$ but rises rapidly to $\sim$10% for $x \sim 0.9$. While the kinematical and R^γ corrections are smaller than the (maximal) d/u effect on the asymmetry, these must be included in the data analysis in order to minimize the uncertainties on the extracted d/u ratio.

In contrast to R^γ, no experimental information currently exists on the interference ratio $R^{\gamma Z}$. Since $R^{\gamma Z}$ enters in the relatively large Y_1 contribution to $A_p^{\rm PV}$, any differences between $R^{\gamma Z}$ and R^γ could have important consequences for the asymmetry. At high Q^2 one expects that $R^{\gamma Z} \approx R^\gamma$ at leading twist, if the PVDIS process is dominated by single quark scattering. At low Q^2, however, since the current conservation constraints are different for weak and electromagnetic probes, there may be significant differences between these.

In Ref. [25] the ratios of σ_L to σ_T cross sections for electromagnetic and weak processes were calculated using a model which combines the low-Q^2 behavior from (axial) vector meson dominance with perturbative QCD constraints at high Q^2 [26]. The resulting ratios R^γ and R^Z (which describes the purely weak Z-exchange contribution) were found to differ by ($<$1%, 17%, 22%) for $x =$ (0.4, 0.6, 0.85) at $Q^2 = 5$ GeV^2. The differences at $Q^2 =$ 10 GeV^2 were ($<$1%, 9%, 23%) for the same x values [27].

For the interference ratio $R^{\gamma Z}$ one may expect qualitatively similar behavior to that of R^γ and R^Z, with $R^{\gamma Z}$ possibly lying in between the purely electromagnetic and weak ratios. However, in the absence of a quantitative determination of $R^{\gamma Z}$, we take a more conservative estimate of the possible differences, and consider a range of possibilities, with R^γ and $R^{\gamma Z}$ differing by 0%, 10%, and 20% for all x.

These are illustrated in Fig. 5, where we plot the ratio $\delta^{(R^{\gamma Z})} A_p^{\rm PV} / A_p^{\rm PV(0)}$, with $\delta^{(R^{\gamma Z})} A_p^{\rm PV}$ the difference between the full asymmetry and that calculated in Bjorken-limit kinematics, $A_p^{\rm PV(0)}$. The baseline correction with $R^{\gamma Z} = R^\gamma$ (dotted curve), equivalent to the solid curve in Fig. 4, with R^γ from Ref. [19], is compared with the effects of modifying $R^{\gamma Z}$ by $\pm 10\%$ (solid curve) and $\pm 20\%$ (dotted-dashed curve). The result of such a modification, which comes through the Y_1 term in the asymmetry, is an $\approx 1\%$ (2%) shift of $A_p^{\rm PV}$ relative to the $R^{\gamma Z}$-independent asymmetry. For $x \lesssim 0.6$, a 20% difference between $R^{\gamma Z}$ and R^γ would be comparable to, or exceed, the maximal d/u uncertainty considered here (dashed curve), although at larger x the sensitivity of $A_p^{\rm PV}$ to d/u becomes increasingly larger. As with the R^γ corrections in Fig. 4, the possible effects on the asymmetry due to $R^{\gamma Z}$ are potentially significant, which warrants further work in understanding the possible differences with R^γ [18].

IV. PVDIS ON THE DEUTERON

In the late 1970s parity-violating DIS on the deuteron provided an important early test of the standard model [1,2]. In the parton model, the asymmetry for an isoscalar

deuteron becomes independent of hadronic structure and is given entirely by electroweak coupling constants. At finite Q^2, however, contributions from longitudinal structure functions, or from higher twist effects, may play a role. The higher twists have been estimated in several phenomenological model studies [16]. More recently, it has been suggested that PVDIS on a deuteron could also be sensitive to charge-symmetry violation (CSV) effects in PDFs (see Ref. [28] for a review of CSV in PDFs). In this section we explore the contributions from kinematical finite-Q^2 effects and the longitudinal structure functions on the PV asymmetry and assess their impact on the extraction of CSV effects.

A. Finite-Q^2 corrections

Assuming the deuteron is composed of a proton and a neutron, and neglecting possible differences between free and bound nucleon PDFs, the functions a_1 and a_3 in Eqs. (18a) and (18b) for a deuteron target become

$$a_1^d = \tfrac{6}{5}(2C_{1u} - C_{1d}), \tag{20a}$$

$$a_3^d = \tfrac{6}{5}(2C_{2u} - C_{2d}). \tag{20b}$$

If in addition $R_d^\gamma \approx R_p^\gamma$ and $R_d^{\gamma Z} \approx R_p^{\gamma Z}$, as is observed experimentally [19], then the y-dependent terms in the deuteron asymmetry become $Y_1^d \approx Y_1^p \equiv Y_1$ and $Y_3^d \approx Y_3^p \equiv Y_3$. The PV asymmetry can then be written as

$$A^{\rm PV} = -\left(\frac{3G_F Q^2}{10\sqrt{2}\pi\alpha}\right)[Y_1(2C_{1u} - C_{1d}) + Y_3(2C_{2u} - C_{2d})], \tag{21}$$

which in the Bjorken limit ($Y_1 \to 1$, $Y_3 \to f(y)$) becomes independent of hadron structure, and is a direct measure of the electroweak coefficients C_{iq}.

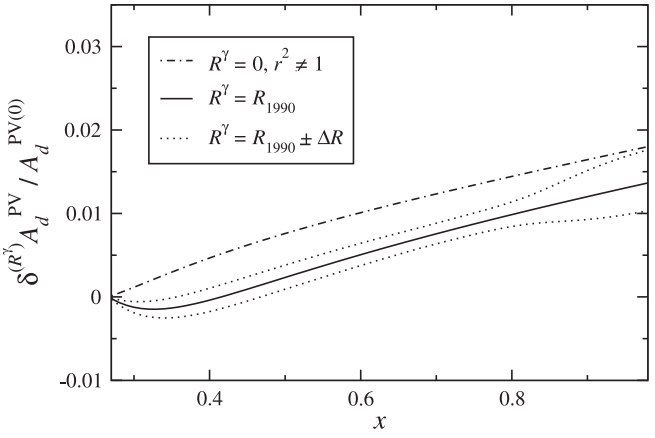

FIG. 6. Relative effects on the deuteron PV asymmetry $A_d^{\rm PV}$ from the electromagnetic ratio R^γ (with $R^{\gamma Z} = R^\gamma$), compared with the Bjorken-limit asymmetry $A_d^{\rm PV(0)}$. The full results (solid curve), for $Q^2 = 5$ GeV^2, are compared with those for $R^\gamma = 0$ (but $r^2 \neq 1$) (dotted-dashed curve), with the dotted curves representing the uncertainty on R^γ (from the R_{1990} parameterization of Ref. [19]).

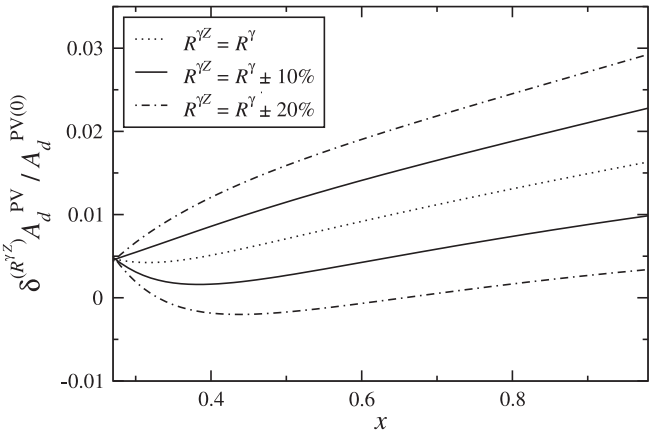

FIG. 7. Relative effects on the deuteron PV asymmetry $A_d^{\rm PV}$ from the γZ interference ratio $R^{\gamma Z}$ compared with the Bjorken-limit asymmetry $A_d^{\rm PV(0)}$. The baseline result for $R^{\gamma Z} = R^\gamma$ (dotted curve) is compared with the effects of modifying $R^{\gamma Z}$ by $\pm 10\%$ (solid curve) and $\pm 20\%$ (dotted-dashed curve), for $Q^2 = 5$ GeV^2.

In Fig. 6 the relative effect on $A_d^{\rm PV}$ from R^γ is shown via the ratio $\delta^{(R^\gamma)} A_d^{\rm PV} / A_d^{\rm PV(0)}$, where $\delta^{(R^\gamma)} A_d^{\rm PV}$ is the difference between the full asymmetry and that calculated in Bjorken-limit kinematics, $A_d^{\rm PV(0)}$. The correction due to R^γ is qualitatively similar to that for the proton asymmetry in Fig. 4, although slightly smaller. The effect on $A_d^{\rm PV}$ from the purely kinematical r^2 correction in the Y_3 term (with $R^\gamma = 0$) is an increase of order 1% over the Bjorken-limit asymmetry in the range $0.5 \lesssim x \lesssim 0.9$. Inclusion of the R^γ ratio cancels the correction somewhat, reducing it to $\lesssim$0%–0.5% for $x \lesssim 0.6$, and to $\lesssim$ 0.5%–1% for $x > 0.6$.

The effects of a possible difference between $R^{\gamma Z}$ and R^γ are illustrated in Fig. 7 through the ratio $\delta^{(R^{\gamma Z})} A_d^{\rm PV} / A_d^{\rm PV(0)}$, where $\delta^{(R^{\gamma Z})} A_p^{\rm PV}$ is the difference between the full and Bjorken-limit asymmetries. As for the proton in Fig. 5, the baseline correction with $R^{\gamma Z} = R^\gamma$ (dotted curve) is compared with the effects of modifying $R^{\gamma Z}$ by a constant $\pm 10\%$ (solid curve) and $\pm 20\%$ (dotted-dashed cruve). This conservative range is, as for the proton, motivated by the phenomenological study of R^γ and R^Z in Ref. [25], and the relatively weak isospin dependence of R^γ [19,20]. This results in an additional $\approx 0.5\%$ (1%) shift of $A_d^{\rm PV}$ for a 10% (20%) modification relative to the baseline asymmetry for $x > 0.5$. Such effects will need to be accounted for if one wishes to compare with the standard model predictions, or when extracting CSV effects in PDFs, which we discuss in the next section.

B. Charge-symmetry violation

In the entire discussion above an implicit assumption has been made that charge symmetry is exact, namely, that the

quark distributions in the proton and neutron are related by $u^p = d^n$ and $u^n = d^p$. Quark mass differences and electromagnetic effects are expected, however, to give rise to (small) violations of charge symmetry in PDFs, which may be parameterized by

$$\delta u = u^p - d^n, \tag{22a}$$
$$\delta d = d^p - u^n. \tag{22b}$$

Nonzero values of δu and δd have been predicted in nonperturbative models of the nucleon [29] and can in addition arise from radiative QED effects in Q^2 evolution [30–32].

It is convenient to define the u and d quark distributions in the presence of CSV according to [33]:

$$u \equiv u^p - \frac{\delta u}{2} = d^n + \frac{\delta u}{2}, \tag{23a}$$
$$d \equiv d^p - \frac{\delta d}{2} = u^n + \frac{\delta d}{2}. \tag{23b}$$

With these definitions, the deuteron functions a_1^d and a_3^d in the $A_d^{\rm PV}$ asymmetry can be written

$$a_1^d = a_1^{d(0)} + \delta^{(\rm CSV)} a_1^d, \tag{24a}$$
$$a_3^d = a_3^{d(0)} + \delta^{(\rm CSV)} a_3^d, \tag{24b}$$

where $a_1^{d(0)}$ and $a_3^{d(0)}$ are given by Eqs. (20a) and (20b), respectively. The fractional CSV corrections are given by

$$\frac{\delta^{(\rm CSV)} a_1^d}{a_1^{d(0)}} = \left(-\frac{3}{10} + \frac{2C_{1u} + C_{1d}}{2(2C_{1u} - C_{1d})}\right)\left(\frac{\delta u - \delta d}{u + d}\right), \tag{25a}$$
$$\frac{\delta^{(\rm CSV)} a_3^d}{a_3^{d(0)}} = \left(-\frac{3}{10} + \frac{2C_{2u} + C_{2d}}{2(2C_{2u} - C_{2d})}\right)\left(\frac{\delta u - \delta d}{u + d}\right). \tag{25b}$$

In Fig. 8 we plot the effect of CSV in valence PDFs on the deuteron asymmetry $A_d^{\rm PV}$. The asymmetry using the MRSTQED parametrization [31] of $\delta u - \delta d$ (solid curve) gives an $\approx 0.5\%$–1% effect for $0.5 \lesssim x \lesssim 0.9$, similar to the effect predicted from nonperturbative (bag model) calculations [29]. The phenomenological fit [30] $\delta u - \delta d = 2\kappa f(x)$, with $f(x) = x^{-1/2}(1-x)^4(x - 0.0909)$ and κ a free parameter, results in a similar correction to the asymmetry, $\sim 0.5\%$ for most of the x range considered. The best fit gives $\kappa = -0.2$, although the constraints on κ are relatively weak, with values of $\kappa = -0.8$ and $+0.65$ giving $\sim 1.5\%$–2% effect for $0.5 \lesssim x \lesssim 0.8$ at the 90% confidence level.

For the central values (best fit parameters), the magnitude of the CSV effect on the asymmetry at $Q^2 = 5$ GeV^2 is similar to that due to the finite-Q^2 kinematics ($r^2 \neq 1$, $R^\gamma \neq 0$) seen in Fig. 6 and may be smaller than that due to possible differences between $R^{\gamma Z}$ and R^γ in Fig. 7. Unless the finite-Q^2 corrections are known to greater accuracy than at present, they may impede the unambiguous extraction of CSV effects from the asymmetry.

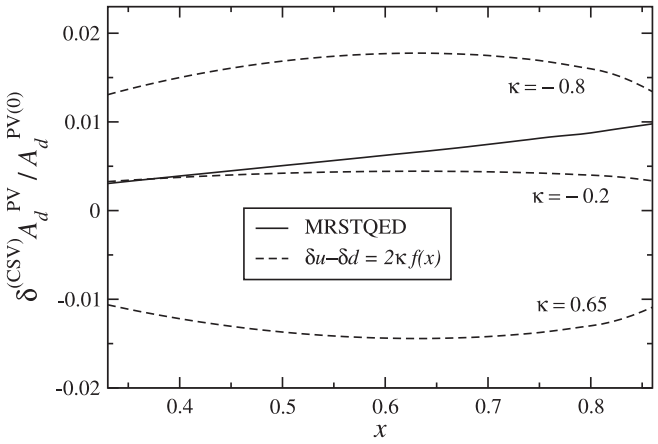

FIG. 8. Relative effects on the deuteron PV asymmetry $A_d^{\rm PV}$ of CSV in PDFs, compared with the charge symmetric asymmetry. The CSV distributions $\delta u - \delta d$ are from the MRSTQED fit [31] (solid curve) and from the parametrization $\delta u - \delta d = 2\kappa f(x)$ (dashed curve, see text), with $\kappa = -0.2$ (best fit), and the two 90% confidence levels, $\kappa = -0.8$ and $\kappa = +0.65$ [30].

On the other hand, since the finite-Q^2 corrections are expected to decrease with Q^2, while the CSV effects are leading twist effects, a cleaner separation should be possible at larger Q^2. In Fig. 9 the effect of R^γ on $A_d^{\rm PV}$ (solid curve) is compared with the CSV results [30] for different κ values (dashed curve) at $Q^2 = 10$ GeV^2. The deviation from the Bjorken-limit kinematics of the $\delta^{(R^\gamma)}$ curve is clearly less than the corresponding result at $Q^2 = 5$ GeV^2 in Fig. 6 (the shaded region here indicates the uncertainty in R^γ), whereas the CSV results are similar to those at the lower Q^2. The contrast is especially striking at $x \sim 0.6$, where the CSV effects are several times larger than the correction to $A_d^{\rm PV}$ due to R^γ. At larger x the CSV

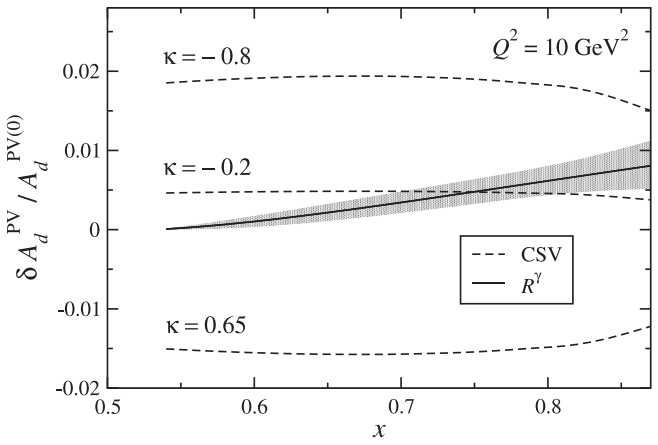

FIG. 9. Relative effects on the deuteron PV asymmetry $A_d^{\rm PV}$ from CSV in PDFs [30] (dashed curve, see Fig. 8) and from R^γ [19] (with $R^{\gamma Z} = R^\gamma$, solid curve) at $Q^2 = 10$ GeV^2, compared with the charge symmetric asymmetry in Bjorken-limit kinematics. The shaded area represents the uncertainty in R^γ.

effects for the central κ value become comparable to the R^γ uncertainty; however, the 90% confidence level corrections ($\kappa = -0.8$ and $+0.65$) are of the order 2% and are still several times larger than the R^γ uncertainty.

These results suggest that if the CSV effects in PVDIS from the deuteron are of the order $\sim$0.5%, the optimal value of x to observe them would be $x \sim 0.6$ at $Q^2 = 10$ GeV^2. If the CSV effects are of order $\sim$2%, they should be clearly visible over a larger x range, even up to $x \approx 0.8$. Note that the minimum value of x attainable at the $Q^2 = 10$ GeV^2 kinematics ($x \approx 0.53$) is somewhat smaller than at the lower Q^2 vales because at fixed incident energy and Q^2 the fractional lepton energy loss exceeds unity at higher x.

V. PROSPECTS FOR PVDIS ON POLARIZED HADRONS

In this section we explore the possibility of extracting *spin-dependent* PDFs in parity-violating unpolarized-electron scattering from a *polarized* hadron. In particular, we examine the sensitivity of the polarized proton, neutron and deuteron PVDIS asymmetries to the polarized Δu and Δd distributions at large x, where these are poorly known. The Δd distribution, in particular, remains essentially unknown beyond $x \approx 0.6$.

The PV differential cross section (with respect to the variables x and y) for unpolarized electrons on longitudinally polarized nucleons can generally be written in terms of 5 spin-dependent structure functions [13]:

$$\frac{d^2\sigma^{\rm PV}}{dxdy}(\bar\lambda, S_L) = 2x\left(2 - y - \frac{xyM}{E}\right)g_1^{\gamma Z} - \frac{4x^2M}{E}g_2^{\gamma Z} + \frac{2}{y}\left(1 - y - \frac{xyM}{2E}\right)g_3^{\gamma Z} - \frac{2}{y}\left(1 + \frac{xM}{E}\right)\left(1 - y - \frac{xyM}{2E}\right)g_4^{\gamma Z} + 2xy\left(1 + \frac{xM}{E}\right)g_5^{\gamma Z}, \tag{26}$$

where the nucleon (longitudinal) spin vector S_L is given by $S_L^\mu = (0; 0, 0, 1)$, and $\bar\lambda$ is the average over $\lambda = +1$ and $\lambda = -1$ [see Eq. (4)]. The analog of the PV asymmetry in Eq. (8) for a polarized target can be defined as

$$\Delta A^{\rm PV} = \frac{\sigma^{\rm PV}(\bar\lambda, S_L) - \sigma^{\rm PV}(\bar\lambda, -S_L)}{\sigma^{\rm PV}(\bar\lambda, S_L) + \sigma^{\rm PV}(\bar\lambda, -S_L)}, \tag{27}$$

where $\sigma^{\rm PV}(\bar\lambda, S_L) \equiv d^2\sigma^{\rm PV}/dxdy$. Some of the structure functions $g_{1-5}^{\gamma Z}$ have simple parton model interpretations, while others do not. At present there is no phenomenological information about these structure functions. In order to proceed, we shall therefore consider the asymmetry in the high energy limit, $M/E \to 0$, which eliminates the structure function $g_2^{\gamma Z}$. In this limit, the operator product expansion gives rise to the relation $g_3^{\gamma Z} - g_4^{\gamma Z} = 2xg_5^{\gamma Z}$, which further eliminates one of the functions. Furthermore, in the parton model the $g_4^{\gamma Z}$ structure function vanishes, leaving the Callan-Gross-like relation $g_3^{\gamma Z} = 2xg_5^{\gamma Z}$. In terms of the remaining two structure functions, the spin-dependent PV asymmetry can be written:

$$\Delta A^{\rm PV} = \frac{G_F Q^2}{4\sqrt{2}\pi\alpha}\left(g_A^e f(y)\frac{g_1^{\gamma Z}}{F_1^\gamma} + g_V^e\frac{g_5^{\gamma Z}}{F_1^\gamma}\right), \tag{28}$$

where the kinematical factor $f(y)$ is given in Eq. (14b).

In the QCD parton model the $g_1^{\gamma Z}$ and $g_5^{\gamma Z}$ structure functions can be expressed in terms of helicity dependent PDFs Δq as [13]

$$g_1^{\gamma Z} = \sum_q e_q g_V^q(\Delta q + \Delta\bar q), \tag{29a}$$

$$g_5^{\gamma Z} = \sum_q e_q g_A^q(\Delta q - \Delta\bar q), \tag{29b}$$

where Δq is a function of x and Q^2. Using these expressions, the PV asymmetries for proton, neutron, and deuteron (which in this analysis we take to be a sum of proton and neutron) targets can then be written [33]

$$\Delta A_p^{\rm PV} = \frac{6G_F Q^2}{4\sqrt{2}\pi\alpha}[(2C_{1u}\Delta u - C_{1d}\Delta d)f(y) + (2C_{2u}\Delta u - C_{2d}\Delta d)]\left(\frac{1}{4u + d}\right), \tag{30a}$$

$$\Delta A_n^{\rm PV} = \frac{6G_F Q^2}{4\sqrt{2}\pi\alpha}[(2C_{1u}\Delta d - C_{1d}\Delta u)f(y) + (2C_{2u}\Delta d - C_{2d}\Delta u)]\left(\frac{1}{u + 4d}\right), \tag{30b}$$

$$\Delta A_d^{\rm PV} = \frac{3G_F Q^2}{10\sqrt{2}\pi\alpha}[(2C_{1u} - C_{1d})f(y) + 2C_{2u} - C_{2d}] \times \left(\frac{\Delta u + \Delta d}{u + d}\right). \tag{30c}$$

Generalizations to higher order are straightforward, however, just as in the unpolarized case; care should be taken with large-x resummations [17], which could modify some of the quantitative conclusions at $x \sim 1$.

In Fig. 10 we illustrate the sensitivity of the proton asymmetry $\Delta A_p^{\rm PV}$ to the Δu and Δd PDFs, by comparing the difference $\delta\Delta A_p^{\rm PV}$ in the asymmetry arising from different parametrizations [34–36], relative to the LSS parametrization [37]. The effects at intermediate x, $x \sim 0.5$–0.6, are of order 20%; however, these increase rapidly with x. At $x \approx 0.7$–0.8 the AAC [35], DNS [36], and LSS [37] parametrizations give asymmetries that are within $\sim$20% of each other, whereas the BB fit [34] deviates by 50%–100% in this range. The results for neutron and deuteron targets are found to be very similar to those in Fig. 10. While this does not constitute a systematic error on the uncertainty in $\Delta A_p^{\rm PV}$ due to PDFs, it does indicate the sensitivity of polarized PVDIS to helicity distributions at

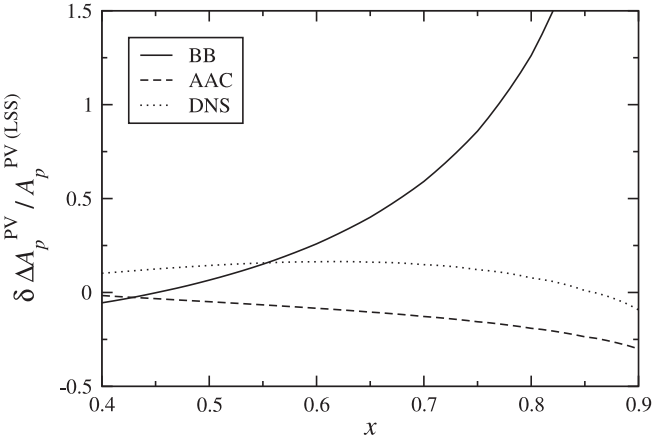

FIG. 10. Sensitivity of the polarized proton PV asymmetry $\Delta A_p^{\rm PV}$ on the spin-dependent Δu and Δd distributions. The asymmetries for the BB [34] (solid curve), AAC [35] (dashed curve), and DNS [36] (dotted curve) distributions are evaluated relative to the baseline asymmetry for the LSS PDFs [37].

large x and suggests that a measurement of $\Delta A_p^{\rm PV}$ at the 10%–20% level could discriminate between different PDF behaviors.

VI. CONCLUSIONS

Parity-violating deep inelastic scattering provides a unique tool with which to study novel aspects of the partonic structure of the nucleon, such as the flavor dependence of PDFs in the region $x \sim 1$ or charge-symmetry violation in PDFs, or even more exotic physics beyond the standard model. In this paper we have examined the sensitivity of the PVDIS process to finite-Q^2 effects which can give rise to important corrections to parton model results at scales $Q^2 \sim$ few GeV^2.

The suppression of the leptonic vector couplings C_{2q} relative to the axial-vector couplings C_{1q} leads to the dominance of the parity-violating asymmetry $A^{\rm PV}$ by the hadronic-vector term a_1. In practice the hadronic a_3 axial-vector contribution amounts to some 20% of the total, for both proton and deuteron targets, and must be accounted for in quantitative numerical analyses. In particular, the a_3 term is associated with the kinematical dependence on the ratio R^γ of electromagnetic longitudinal to transverse photon cross sections.

For the proton asymmetry, which is sensitive to the d/u parton distribution function ratio at large x [7], the corrections from nonzero values of $r^2 - 1 = \frac{4M^2x^2}{Q^2}$ and R^γ lead to an $\approx$ 1%–2% shift in $A_p^{\rm PV}$ over the range $0.6 \lesssim x \lesssim 0.8$, with an uncertainty of $\pm 0.5\%$, increasing to an $\approx 3\%$ shift for $x \approx 0.9$ with an uncertainty of $\pm 1\%$. This is to be compared with a sensitivity ranging from $\approx$ 3%–10% in the asymmetry due to different behaviors of the d/u ratio for the same range of x.

The correction from the longitudinal to transverse γ-Z interference cross section ratio $R^{\gamma Z}$, which has an unexplored phenomenology, could contribute to $A_p^{\rm PV}$ if it differs significantly from R^γ, especially given that $R^{\gamma Z}$ enters through the large, C_{1q}-weighted vector term. While we expect that $R^{\gamma Z} \approx R^\gamma$ at high Q^2, deviations of 10% (20%) at $Q^2 \sim 5$ GeV^2 would result in $\approx 1\%(2\%)$ shift in the asymmetry. For $x \lesssim 0.6$ this would be comparable to the maximal d/u effect on $A_p^{\rm PV}$, although at larger x the sensitivity to d/u becomes increasingly larger.

For the deuteron asymmetry, the low-Q^2 corrections due to r^2 and R^γ are similar to those for the proton at $Q^2 =$ 5 GeV^2, although slightly smaller, and lead to an increase of $\lesssim 1\%$ in the Bjorken-limit asymmetry for $x \lesssim 0.85$. Possible deviations of $R^{\gamma Z}$ from R^γ can lead to further corrections to $A_d^{\rm PV}$, ranging from $\approx$ 0.5%–1% for 10%–20% differences between the ratios. Such effects are comparable with those arising from charge-symmetry violation in PDFs, as estimated in nonperturbative models and phenomenological fits to data. This suggests that without better knowledge of the low-Q^2 corrections, and $R^{\gamma Z}$ in particular, extracting unambiguous information on CSV at these kinematics may be difficult. On the other hand, since the CSV effects on PDFs are leading twist, they will persist at larger Q^2 where the corrections due to $R^{\gamma(\gamma Z)}$ will be suppressed. A cleaner separation of the CSV effects should therefore be more feasible at larger Q^2, $Q^2 \approx 10$ GeV^2, where the CSV effects can be up to several times larger than those due to finite longitudinal cross sections. The proposed experiments at JLab with 12 GeV [4] plan to measure the PV asymmetries over a wide range of Q^2 and y at fixed values of x, which should enable the various effects to be disentangled.

Finally, we have explored the possibility of constraining spin-dependent PDFs from PVDIS of unpolarized leptons from polarized hadrons. Currently there is considerable uncertainty in the behavior of the Δu and Δd helicity distributions at large x, and our estimates suggest that, while challenging, measurement of polarized PV asymmetries at the 10%–20% level could discriminate between different PDF behaviors for $x > 0.7$. Whether this can be achieved experimentally in the foreseeable future remains to be seen [38].

For the future, a number of outstanding issues can be identified. First, the present exploratory studies need to be complemented by more quantitative determinations of $R^{\gamma Z}$, either from model calculations or from phenomenology, in order to reduce the uncertainties in the low-Q^2 corrections to the asymmetries. In addition, target mass corrections to the interference structure functions $F_{1-3}^{\gamma Z}$ should be computed, which may have important consequences in the large-x, low-Q^2 region [15]. Furthermore, the effects of higher twist contributions to electroweak structure functions must be taken into account; although these have been estimated in nonperturbative models to be relatively small [16], they nonetheless need to be included in a complete analysis of PVDIS at few-GeV^2 scales. The

work presented here sets the stage for more detailed theoretical analysis [18] in the run-up to future precision PVDIS measurements at facilities such as Jefferson Lab [3,4].

ACKNOWLEDGMENTS

We thank K. S. Kumar, J. T. Londergan, K. Paschke, P. Reimer, P. Souder, and X. Zheng for helpful discussions and communications, and S. A. Kulagin for sending the results of Ref. [25]. T. H. thanks the U. S. Department of Energy's Science Undergraduate Laboratory Internships (SULI) Program at Jefferson Lab and the Jefferson Lab Theory Center for support. This work was supported by the DOE Contract No. DE-AC05-06OR23177, under which Jefferson Science Associates, LLC operates Jefferson Lab.

[1] C. Y. Prescott *et al.*, Phys. Lett. **77B**, 347 (1978); C. Y. Prescott *et al.*, Phys. Lett. **84B**, 524 (1979).
[2] R. N. Cahn and F. J. Gilman, Phys. Rev. D **17**, 1313 (1978).
[3] Jefferson Lab experiment E-05-007, R. Michaels, P. Reimer, and X. Zheng spokespersons; Jefferson Lab experiment E12-07-102, K. Paschke, P. Reimer, and X. Zheng spokespersons.
[4] P. Souder, talk given at the Workshop on Inclusive and Semi-Inclusive Spin Physics with High Luminosity and Large Acceptance at 11 GeV, Jefferson Lab, Dec. 13–14, 2006; K. S. Kumar, 15th International Workshop on Deep-Inelastic Scattering and Related Subjects (DIS2007), Munich, Germany, Apr. 16–20, 2007.
[5] W. M. Yao *et al.* (Particle Data Group), J. Phys. G **33**, 1 (2006).
[6] J. D. Bjorken, Phys. Rev. D **18**, 3239 (1978).
[7] P. A. Souder, AIP Conf. Proc. **747**, 199 (2005).
[8] SLAC proposal E-149 (1992), P. E. Bosted spokesperson.
[9] W. Melnitchouk and A. W. Thomas, Phys. Lett. B **377**, 11 (1996).
[10] I. R. Afnan *et al.*, Phys. Lett. B **493**, 36 (2000); I. R. Afnan *et al.*, Phys. Rev. C **68**, 035201 (2003).
[11] L. L. Frankfurt and M. I. Strikman, Phys. Rep. **76**, 215 (1981); S. Simula, Phys. Lett. B **387**, 245 (1996); W. Melnitchouk, M. Sargsian, and M. I. Strikman, Z. Phys. A **359**, 99 (1997); Jefferson Lab experiment E03-012, S. Kuhn *et al.* spokespersons.
[12] W. Melnitchouk, I. R. Afnan, F. R. P. Bissey, and A. W. Thomas, Phys. Rev. Lett. **84**, 5455 (2000).
[13] M. Anselmino, P. Gambino, and J. Kalinowski, Z. Phys. C **64**, 267 (1994). Note that the electroweak couplings used here differ by a factor of 2 relative to those of Ref. [5], $C_{iq} = 2C_{iq}^{\text{Anselmino}}$.
[14] A. W. Thomas and W. Weise, *The Structure of the Nucleon* (Wiley-VCH, Berlin, Germany, 2001).
[15] I. Schienbein *et al.*, J. Phys. G **35**, 053101 (2008).
[16] S. Fajfer and R. J. Oakes, Phys. Rev. D **30**, 1585 (1984); P. Castorina and P. J. Mulders, Phys. Rev. D **31**, 2760 (1985); M. Dasgupta and B. R. Webber, Phys. Lett. B **382**, 273 (1996); E. Stein *et al.*, Phys. Lett. B **376**, 177 (1996); A. I. Signal, Nucl. Phys. **B497**, 415 (1997); E. Stein *et al.*, Nucl. Phys. **B536**, 318 (1998); M. Beneke, Phys. Rep. **317**, 1 (1999).
[17] G. Corcella and L. Magnea, Phys. Rev. D **72**, 074017 (2005).
[18] T. Hobbs *et al.* (unpublished).
[19] L. W. Whitlow *et al.*, Phys. Lett. B **250**, 193 (1990).
[20] K. Abe *et al.*, Phys. Lett. B **452**, 194 (1999).
[21] M. E. Christy *et al.* (unpublished).
[22] W. K. Tung *et al.*, J. High Energy Phys. 02 (2007) 053.
[23] W. Melnitchouk and J. C. Peng, Phys. Lett. B **400**, 220 (1997).
[24] G. R. Farrar and D. R. Jackson, Phys. Rev. Lett. **35**, 1416 (1975).
[25] S. A. Kulagin and R. Petti, Phys. Rev. D **76**, 094023 (2007).
[26] S. Alekhin, K. Melnikov, and F. Petriello, Phys. Rev. D **74**, 054033 (2006).
[27] S. A. Kulagin (private communication).
[28] J. T. Londergan and A. W. Thomas, Prog. Part. Nucl. Phys. **41**, 49 (1998); J. T. Londergan and A. W. Thomas, J. Phys. G **31**, 1151 (2005).
[29] E. Sather, Phys. Lett. B **274**, 433 (1992); J. T. Londergan *et al.*, Phys. Lett. B **340**, 115 (1994); C. Boros, F. M. Steffens, J. T. Londergan, and A. W. Thomas, Phys. Lett. B **468**, 161 (1999).
[30] A. D. Martin, R. G. Roberts, W. J. Stirling, and R. S. Thorne, Eur. Phys. J. C **35**, 325 (2004).
[31] A. D. Martin, R. G. Roberts, W. J. Stirling, and R. S. Thorne, Eur. Phys. J. C **39**, 155 (2005).
[32] M. Gluck, P. Jimenez-Delgado, and E. Reya, Phys. Rev. Lett. **95**, 022002 (2005).
[33] K. S. Kumar (private communication).
[34] J. Bluemlein and H. Bottcher, Nucl. Phys. **B636**, 225 (2002).
[35] M. Hirai, S. Kumano, and N. Saito (Asymmetry Analysis Collaboration), Phys. Rev. D **69**, 054021 (2004).
[36] D. de Florian, G. A. Navarro, and R. Sassot, Phys. Rev. D **71**, 094018 (2005).
[37] E. Leader, A. V. Sidorov, and D. B. Stamenov, Phys. Rev. D **73**, 034023 (2006).
[38] X. Zheng, JLab Technical Note JLAB-TN-08-004.